Nuclear Magnetic Resonance in Antiferromagnetic $Rb_2MnCl_4 \cdot 2H_2O$ and $Cs_2MnCl_4 \cdot 2H_2O$†

R. D. SPENCE, J. A. CASEY, AND V. NAGARAJAN
Department of Physics, Michigan State University, East Lansing, Michigan 48823
(Received 2 December 1968)

The NMR spectra of H, Cl, Rb, or Cs nuclei in antiferromagnetic $Rb_2MnCl_4 \cdot 2H_2O$ and $Cs_2MnCl_4 \cdot 2H_2O$ were used to study magnetic ordering in these compounds. The proton resonance data show that the magnetic space group is $P_s\bar{1}$ and that the magnetic unit call is quite different from the chemical unit cell. For the $I > \frac{1}{2}$ nuclei, we have used only the minimum amount of information borrowed from the paramagnetic state to find the direction and magnitude of the internal fields. To do this we have relied on the experimental evaluation of traces and derivatives of traces of the Hamiltonian. The transferred hyperfine field at the two Cl sites in the coordination octhahedron differs by 10% at 1.1°K, and the Mn environment is octahedral only in the zeroth approximation. There appears to be no great difference in the amount of unpaired spin transferred to the Cl sites in the two compounds. Appreciable hyperfine fields are found at the Rb and Cs sites. The hyperfine field at the Cs site is larger than that at the Rb site, and it is suggested that this may have somewhat inhibited the decrease of T_N arising from increased Mn-Mn distances when Rb is replaced with Cs.

I. INTRODUCTION

RECENTLY, specific heat,[1,2] susceptibility,[3] and nuclear-magnetic-resonance[4] studies of $Rb_2MnCl_4 \cdot 2H_2O$ and $Cs_2MnCl_4 \cdot 2H_2O$ have shown that these substances order antiferromagnetically with Néel temperatures of $T_N = 2.24$°K and $T_N = 1.84$°K, respectively. The susceptibility studies indicate a simple uniaxial antiferromagnetism with a very large anisotropy energy. Interest in the magnetic behavior of these crystals stems from the fact that their structures are quite simple compared to most crystals which order magnetically at low temperatures. Each unit cell (see Fig. 1) contains only one molecular unit and thus only one magnetic ion. The space group is $P\bar{1}$ and the lattice parameters[5] are given in Table I.

The present paper reports a study of the hydrogen, chlorine, rubidium, and cesium nuclear resonance in the antiferromagnetic state of these compounds. We restrict ourselves to those results which seem to have bearing on their magnetic structure. It appears that the nuclear-resonance data enables us to specify the antiferromagnetic spin arrangement and to suggest the source of the modification of the exchange constants responsible for the large difference in Néel temperatures in these two crystals.

II. INTERNAL FIELDS

The internal magnetic fields found in magnetically ordered materials may be measured quite directly at the nuclear sites for which the nuclear-resonance experiment is possible. In this section, we collect certain mathematical results which are useful in the calculation and characterization of the internal magnetic fields observed in our experiments.

The Hamiltonian of a proton in an internal magnetic field $\mathbf{B}$ is given by

$$\mathcal{H} = -\gamma_p \hbar \mathbf{I} \cdot \mathbf{B} + \mathcal{H}_d. \quad (1)$$

The nuclear dipole-dipole term $\mathcal{H}_d$ leads to two symmetrically disposed lines whose average frequency $\bar{\nu}$ is related to the internal field by

$$B = (2\pi/\gamma_p)\bar{\nu}. \quad (2)$$

For $I > \frac{3}{2}$ the dipole-dipole term (in the present case) is quite negligible, but the quadrupole term is very important. Thus for $I > \frac{3}{2}$,

$$\mathcal{H} = -\gamma_n \hbar \mathbf{I} \cdot \mathbf{B} + \mathbf{Q} : \nabla \mathbf{E}, \quad (3)$$

where $\mathbf{Q} = \mathbf{Q}(I)$ is the quadrupole tensor matrix and $\nabla \mathbf{E}$ is the electric-field-gradient tensor. The eigenvalues of the Hamiltonian are given by the roots of the secular

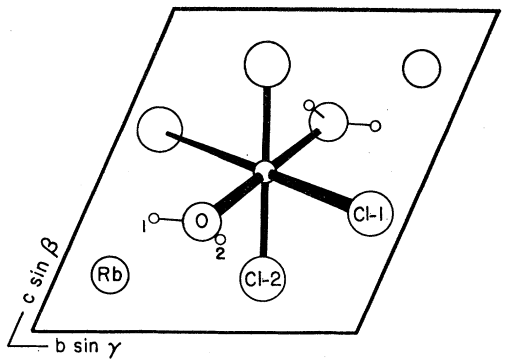

FIG. 1. Chemical cell of $Rb_2MnCl_4 \cdot 2H_2O$. The cell for $Cs_2MnCl_4 \cdot 2H_2O$ is obtained by replacing Rb ions with Cs ions.

† Research was sponsored by the Air Force Office of Scientific Research, Office of Aerospace Research, U. S. Air Force.
[1] H. Forstat, N. D. Love, and J. N. McElearney, Phys. Letters **25A**, 253 (1967).
[2] H. Forstat, N. D. Love, and J. N. McElearney, Bull. Am. Phys. Soc. **12**, 285 (1967).
[3] T. Smith and S. A. Friedberg (unpublished).
[4] R. D. Spence, J. A. Casey, and V. Najarajan, Bull. Am. Phys. Soc. **12**, 58 (1967).
[5] S. J. Jensen, Acta Chem. Scand. **18**, 2085 (1964).

TABLE I. Cell dimensions and interaxial angles.

	$Rb_2MnCl_4\cdot 2H_2O$	$Cs_2MnCl_4\cdot 2H_2O$
a (Å)	5.66±0.01	5.74±0.01
b (Å)	6.48±0.01	6.66±0.01
c (Å)	7.01±0.01	7.27±0.01
α	66.7°±0.1°	67.0°±0.1°
β	87.7°±0.1°	87.8°±0.1°
γ	84.8°±0.1°	84.3°±0.1°

equation

$$\lambda^{2I+1}-\tfrac{1}{2}\Gamma_2\lambda^{2I}-\tfrac{1}{3}\Gamma_3\lambda^{2I-1}+\cdots+D=0, \quad (4)$$

where

$$\Gamma_n=\mathrm{Tr}(\mathfrak{IC})^n \quad (5a)$$

and

$$D=\det\mathfrak{IC}. \quad (5b)$$

Each Γ_n consists of a linear combination of the nth-order scalars which can be constructed from the vector $\mathbf{B}$ and the tensor $\nabla\mathbf{E}$. The coefficients of the various terms in a given Γ_n can only contain γ_n, $\hbar$, eQ, and I. Expressed in frequency units[6]

$$\Gamma_2=a_1(\gamma_n/2\pi)^2B^2+a_2\nu_Q^2(1+\tfrac{1}{3}\eta^2) \quad (6)$$

and

$$\Gamma_3=a_3\nu_Q(\gamma_n/2\pi)^2B^2(3\cos^2\theta-1+\eta\sin^2\theta\cos2\varphi)+a_4\nu_Q^3(1-\eta^2). \quad (7)$$

Here θ and φ represent the polar and azimuthal angles of $\mathbf{B}$ with respect to the X, Y, and Z axes of the electric-field-gradient tensor. The elements of $\nabla\mathbf{E}$ are specified by $q=\partial E_Z/\partial Z$ and $\eta=\{\partial E_X/\partial X-\partial E_Y/\partial Y\}/q$ and the quantity $\nu_Q=e^2qQ/2h$. The coefficients a_i for $I=\frac{3}{2}$, $\frac{5}{2}$, and $\frac{7}{2}$ are given in Table II. Higher-order Γ_n tend to be rather complicated. For $I=\frac{3}{2}$ one finds for Γ_4 and D,

$$\Gamma_4=(\tfrac{41}{4})(\gamma_n/2\pi)^4B^4+(\gamma_n/2\pi)^2\nu_Q^2[\tfrac{9}{2}+3\cos^2\theta-2\eta\sin^2\theta\cos2\varphi+\eta^2(7/6+\sin^2\theta)]+(\nu_Q^4/144)(3+\eta^2)^2, \quad (8)$$

$$D=\tfrac{1}{8}[(\Gamma_2)^2-2\Gamma_4]. \quad (9)$$

Using the fact that $\Gamma_1=0$ one may also express the Γ_n as nth-order polynomials in the observed frequencies. Thus, for example, for Γ_2 one finds

$$\Gamma_2=(1/2I+1)^2\sum_{n=0}^{2I}\sum_{i=1}^{2I}\sum_{j=1}^{2I}c_i(n)c_j(n)\nu_i\nu_j, \quad (10)$$

TABLE II. Coefficients for calculating Γ_n.

Coefficient	$I=\frac{3}{2}$	$I=\frac{5}{2}$	$I=\frac{7}{2}$
a_1	5	35/2	42
a_2	1	21/25	6/7
a_3	3	42/5	18
a_4	0	3/25	48/343

[6] L. C. Brown and P. M. Parker, Phys. Rev. **100**, 1764 (1955).

where

$$c_k(n)=k\cdots k\leq n \quad (11)$$

and

$$c_k(n)=k-(2I+1)\cdots k>n. \quad (12)$$

In the *paramagnetic* state the internal field averages to zero and the appropriate formulas for Γ_2, Γ_3, Γ_4 are found by setting B to zero in Eqs. (6)–(8). The experimental values for Γ_2, Γ_3, Γ_4 in the paramagnetic state can be found from the pure quadrupole frequencies. Combining the results of the antiferromagnetic and paramagnetic states gives the magnitude of the internal field in the antiferromagnetic state as

$$B^2=[(2\pi/\gamma_n)^2/a_1](\Gamma_2{}^a-\Gamma_2{}^p), \quad (13)$$

where the superscripts a and p refer to the antiferromagnetic and paramagnetic states. The problem of determining the orientation of the internal fields is more complicated. One may measure the orientation of the axes of the tensor $\nabla\mathbf{E}$ and the value of η in the paramagnetic state by using some standard technique such as the "elliptical cone" method.[7] The orientation of $\mathbf{B}$ with respect to the axes of $\nabla\mathbf{E}$ is then found using Eqs. (7) and (8). As an alternative one may apply a small external field $\delta\mathbf{H}$ with the crystal in the *antiferromagnetic* state. The shift in the frequency ν_i is then given by

$$\delta\nu_i=\nabla_H\nu_i\cdot\delta\mathbf{H}, \quad (14a)$$

where

$$\nabla_H=\mathbf{i}\frac{\partial}{\partial H_x}+\mathbf{j}\frac{\partial}{\partial H_y}+\mathbf{k}\frac{\partial}{\partial H_z}. \quad (14b)$$

Here x, y, z and the associated unit vectors $\mathbf{i}$, $\mathbf{j}$, $\mathbf{k}$ refer to any convenient set of rectangular axes. Applying the operator ∇_H to Eqs. (6) and (10) gives the vector

$$\mathbf{G}_2\equiv\nabla_H\Gamma_2=\mathbf{B}\cdot\mathbf{T}=[[2\pi/\gamma_n(2I+1)]^2/2a_1]\times\sum_{i=1}^{2I}\sum_{j=1}^{2I}c_{ij}\nu_i\nabla_H\nu_j, \quad (15)$$

where

$$c_{ij}=\sum_{n=0}^{2I}c_i(n)c_j(n) \quad (16)$$

and

$$\mathbf{T}=\tfrac{1}{2}[\nabla_HB+(\nabla_HB)_t], \quad (17)$$

where the subscript t indicates the transpose.

The tensor $\mathbf{T}$ may be written

$$\mathbf{T}=\mathbf{I}+\boldsymbol{\sigma}. \quad (18)$$

The tensor $\boldsymbol{\sigma}$ is generally small compared to the unit tensor and therefore $\mathbf{G}_2$ is essentially parallel to $\mathbf{B}$. As will be shown later good approximations for $\boldsymbol{\sigma}$ are available which allow one to determine the orientation of $\mathbf{B}$ even more accurately.

[7] T. P. Das and E. L. Hahn, *Nuclear Quadrupole Resonance Spectroscopy* (Academic Press Inc., New York, 1958), p. 22.

One may also define a vector $\mathbf{G}_3=\nabla_H\Gamma_3$. This is of use if one determines θ, φ, and η from antiferromagnetic data alone. Combined with the expressions for Γ_3 and Γ_4, $\mathbf{G}_3$ provides the required third equation for finding the three unknowns.

Experimentally the measurement of the $\nabla_H\nu_i$ which are required to compute $\mathbf{G}_2$ and $\mathbf{G}_3$ is quite simple. One finds the orientation of the small steady field $\delta\mathbf{H}$ which produces the maximum shift in ν_i. This orientation is the direction of $\nabla_H\nu_i$. The magnitude $|\nabla_H\nu_i|$ is the maximum frequency shift divided by the magnitude of $\delta\mathbf{H}$.

The internal magnetic field $\mathbf{B}(\mathbf{r})$ at a nuclear site whose position vector is $\mathbf{r}$ may be expressed in terms of the semiclassical spatially varying magnetization $\mathbf{M}(\mathbf{r})$ by[8]

$$\mathbf{B}(r)=\frac{8\pi}{3}\mathbf{M}(r)+\int_\epsilon\frac{3\boldsymbol{\varrho}_1\boldsymbol{\varrho}_1-\mathbf{I}}{|\mathbf{r}-\mathbf{r}'|^3}\cdot\mathbf{M}(\mathbf{r}')dr'^3, \tag{19}$$

where the limit ϵ indicates that the point $\mathbf{r}=\mathbf{r}'$ is omitted from the integral and $\boldsymbol{\varrho}_1$ is a unit vector along $\mathbf{r}-\mathbf{r}'$. We divide the field into two parts

$$\mathbf{B}=\mathbf{B}_h+\mathbf{B}_d. \tag{20}$$

The (transferred) hyperfine field $\mathbf{B}_h$ consists of the contact term $\frac{1}{3}8\pi\mathbf{M}$ and that portion of the contribution from the integral which arises from the magnetization (unpaired spin) in the p orbitals of the ion in which the nucleus is imbedded. The dipolar field $\mathbf{B}_d$ arises from the remaining magnetization in the more distant parts of the crystal. Both $\mathbf{B}_h$ and $\mathbf{B}_d$ are linearly related to $\mathbf{M}$ and hence to the magnetic ion's average magnetic moment $\boldsymbol{\mu}$. Hence

$$\mathbf{B}_h=\boldsymbol{\Lambda}\cdot\boldsymbol{\mu} \tag{21}$$

and

$$\mathbf{B}_d=\boldsymbol{\Delta}\cdot\boldsymbol{\mu}. \tag{22}$$

The tensor $\boldsymbol{\Lambda}$ may be expressed in terms of the conventional transferred hyperfine interaction tensors $\mathbf{A}_i$ by

$$\gamma_n\gamma_e\hbar^2\boldsymbol{\Lambda}=\sum_i\vartheta_i\mathbf{A}_i. \tag{23}$$

The sum runs over only the set of *magnetic* ions whose wave functions interact with those of the ion containing the nucleus in question. The quantities $\vartheta_i=\pm1$ are determined by the magnetic space group. Even if $\boldsymbol{\Lambda}$ is known in the antiferromagnetic state, the individual $\mathbf{A}_i$ can not be determined unless all except one vanish or they differ only in a known rotation of axes. If the distribution of magnetization about the magnetic ions is spherically symmetric, we have

$$\boldsymbol{\Delta}=\sum_i\vartheta_i(3\boldsymbol{\varrho}_1\boldsymbol{\varrho}_1-\mathbf{I})/|\mathbf{r}-\mathbf{r}_i'|^3, \tag{24}$$

where the summation extends over all ions of the crystal. Since the ϑ_i are determined by the magnetic space group, nuclei for which $\mathbf{B}_d\gg\mathbf{B}_h$ (e.g., protons in the present case) give details of the spin arrangement in the crystal, whereas nuclei for which $\mathbf{B}_h\gg\mathbf{B}_d$ and for which only one term in Eq. (23) differs from zero can only provide information about the unpaired spin density in their neighborhood.

To obtain the elements of $\boldsymbol{\Lambda}$ from Eq. (21), one must know the axes of $\boldsymbol{\Lambda}$ as well as the vectors $\mathbf{B}_h$ and $\boldsymbol{\mu}$. In the present problem, we are primarily interested only in comparing the hyperfine interaction in two isostructural compounds in a way that is temperature-independent. For this purpose the quantity

$$\Lambda_e=|B_h|/|\mu| \tag{25}$$

is adequate. If $\boldsymbol{\mu}$ is along an axis of $\boldsymbol{\Lambda}$ then $\Lambda_e=\Lambda_{\mu\mu}$, otherwise Λ_e is intermediate in value between the smallest and largest element of $\boldsymbol{\Lambda}$.

Returning to the shift tensor $\boldsymbol{\sigma}$ defined by Eqs. (17) and (18), we note that Eqs. (21) and (22) imply that $\boldsymbol{\sigma}$ has distinct values for the hyperfine and dipolar fields:

$$\boldsymbol{\sigma}_h=\tfrac{1}{2}(\boldsymbol{\chi}\cdot\boldsymbol{\Lambda}'+\boldsymbol{\Lambda}'\cdot\boldsymbol{\chi}), \tag{26}$$

$$\sigma_d=\tfrac{1}{2}(\boldsymbol{\chi}\cdot\boldsymbol{\Delta}'+\boldsymbol{\Delta}'\cdot\boldsymbol{\chi}), \tag{27}$$

where $\boldsymbol{\chi}=\partial\boldsymbol{\mu}/\partial\mathbf{H}$ is the susceptibility tensor (per ion) of the antiferromagnetic state. The primes on $\boldsymbol{\Lambda}$ and $\boldsymbol{\Delta}$ serve to remind one that the application of the field $\delta\mathbf{H}$ produces a *paramagnetic* array of dipoles of moment $\delta\boldsymbol{\mu}$. The primed tensors are obtained by setting $\vartheta_i=1$ in Eqs. (23) and (24). The tensor $\boldsymbol{\sigma}_d$ is generally small compared with the unit tensor. This is not necessarily true of $\boldsymbol{\sigma}_h$ particularly for the Cl nuclei. However, in this case only one hyperfine interaction is important, and one expects the anisotropy of Λ to be much smaller than the anistropy of $\boldsymbol{\chi}$ in the antiferromagnetic state. Hence the vector

$$\mathbf{G}_2=\mathbf{B}_h\cdot(\mathbf{I}+\boldsymbol{\sigma}_h)+\mathbf{B}_d\cdot(\mathbf{I}+\boldsymbol{\sigma}_d) \tag{28}$$

may be approximated by

$$\mathbf{G}_2\simeq\mathbf{B}_h\cdot(\mathbf{I}+\Lambda_e\boldsymbol{\chi})+\mathbf{B}_d. \tag{29}$$

Previous workers[9,10] have often *assumed* that for certain nuclei the axes of $\boldsymbol{\chi}$, $\boldsymbol{\Lambda}$, and $\boldsymbol{\Lambda}'$ (hence $\boldsymbol{\sigma}$ also) are all parallel. In such a case it follows from Eqs. (15), (18), (21), and (26) that $\mathbf{G}_2-\mathbf{B}_d$ and $\mathbf{B}_h$ should be exactly parallel if $\boldsymbol{\sigma}_d$ is negligible. There seems to be no very good reason why this assumption should be precisely valid in crystals of low symmetry such as the present compounds. However, if the anisotropy of $\boldsymbol{\Lambda}$ and $\boldsymbol{\Lambda}'$ is small, the *result* following from the assumption will be approximately correct.

[8] B. Bleaney, in *Hyperfine Interactions*, edited by A. J. Freeman and R. B. Frankel (Academic Press Inc., New York, 1967), Chap. 1.

[9] W. J. O'Sullivan, W. A. Robinson, and W. W. Simmons, Phys. Rev. 124, 1317 (1961).

[10] A. Narath, Phys. Rev. 136, A766 (1964).

III. EXPERIMENTAL

A. Preparation and Detection

The crystals used in the experiments were cut in the form of prolate spheroids with an axial ratio of 3:1 and with the minor axis along the direction of χ_{11} in the antiferromagnetic state. They were mounted on the nuclear-resonance goniometer and their orientation checked by x rays. Following each experiment the goniometer was removed from the He Dewar and the orientation was again checked by x rays.

Both the cryogenic and detection apparatus was of conventional design. The marginal oscillator gave excellent signals of high intensity from all nuclei in the antiferromagnetic state. In the paramagnetic state the signals from the Rb and Cs nuclei were quite satisfactory. However, even in zero field the Cl signals in the paramagnetic state were wide (~70 kc/sec at 4°K) and of low intensity. The application of an external field of any appreciable size reduced their intensity to below the noise level. This unfortunate situation forced us to rely on data of the antiferromagnetic state in determining the *orientation* of the internal fields at the Cl sites. In the following sections we summarize the experimental results for the various nuclei in the two crystals.

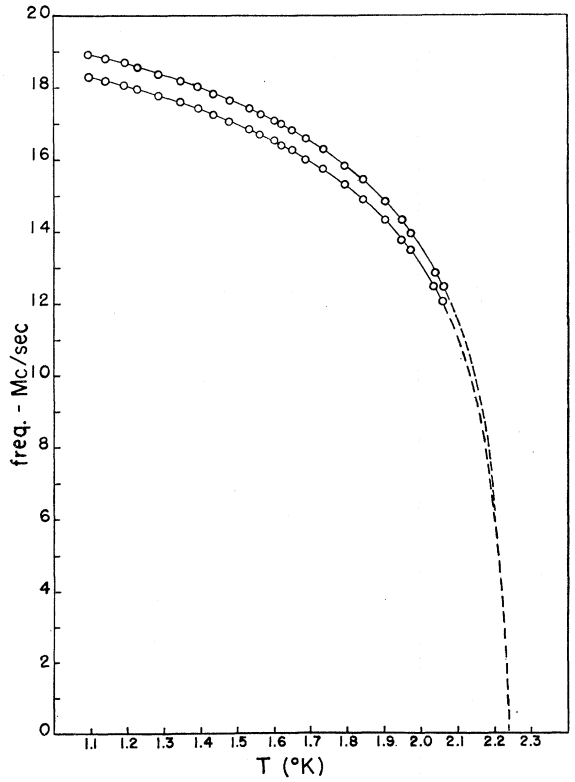

FIG. 2. Temperature dependence of the proton resonance lines in $Rb_2MnCl_4 \cdot 2H_2O$.

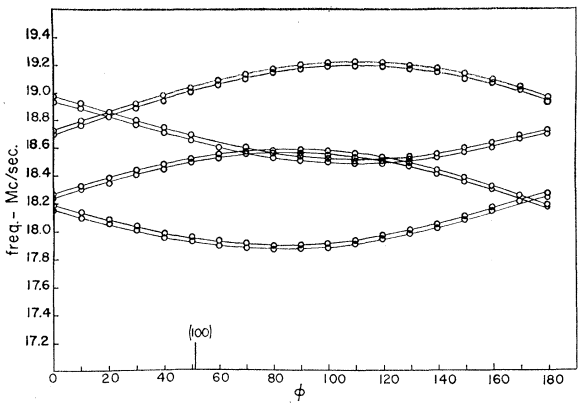

FIG. 3. Resonance diagram for protons of $Rb_2MnCl_4 \cdot 2H_2O$ in an external field of 84 Oe. The rotation axis is the [00$\bar{1}$] zone.

B. Proton Resonance

In both compounds the proton resonance in zero applied field consists of two lines each of which shows a partially resolved nuclear dipole-dipole splitting (~35 kc/sec). The temperature dependence of the frequencies of the two lines is shown for $Rb_2MnCl_4 \cdot 2H_2O$ in Fig. 2. The frequencies of the lines in the two compounds are essentially the same for corresponding values of $T-T_N$. Application of a small field (84 Oe) gives a resonance diagram such as shown in Fig. 3 for $Rb_2MnCl_4 \cdot 2H_2O$. The pattern indicates that the ordering is antiferromagnetic. It also shows that there are no magnetic symmetries other than those which carry a given internal field into an oppositely oriented field. The Mn ion is located at a crystallographic inversion center which is the *only* crystallographic symmetry element in the chemical unit cell. In the magnetic space group,[11] this point must remain an inversion center rather than becoming an antiinversion center, since magnetic moments can not exist at anticenters.[12] Thus the symmetry element responsible for the antiparallel fields shown in Fig. 3 can only be an antitranslation along one edge of the *magnetic* unit cell. A triclinic magnetic cell with an antitranslation along one edge is designated by P_s. Since the cell contains the inversion $\bar{1}$ the magnetic space group is $P_s\bar{1}$.[13] It is important to note that the edges of the magnetic unit cell in the present case are not necessarily parallel to the edges of the chemical unit cell employed for the description of the atomic arrangement of the crystal. However, all the various types of P_s unit cells may be generated by taking either one, two, or three edges of the *chemical* unit cell as antitranslations. To decide which of the seven possible types of P_s unit

[11] W. Opechowski and R. Gucione, in *Magnetism*, edited by G. T. Rado and H. Suhl (Academic Press Inc., New York, 1965), Vol. II A, Chap. 3.

[12] G. Donnay, L. M. Corliss, J. P. H. Donnay, and J. M. Hastings, Phys. Rev. **112**, 1917 (1958).

[13] V. A. Koptsik, *Shubnikov Groups* (Moscow University, 1966).

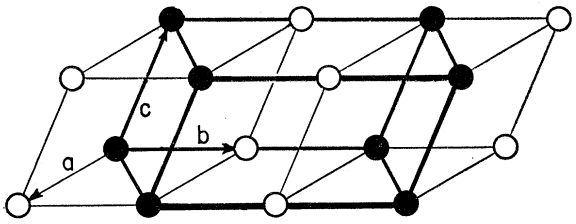

FIG. 4. Relation of the chemical and magnetic unit cells. Chemical cell outlined in light lines. Magnetic cell outlined in heavy lines. Change of color represents a spin reversal.

cells generated by this process correspond to the physical situation one must compare the experimentally observed internal fields with those calculated for each of the seven possibilities.

The magnitude of the internal fields at the proton sites were found from Eq. (2). Their directions were determined by finding the direction along which a small field $\delta\mathbf{H}$ must be applied to produce the maximum shift in the frequency. To calculate the corresponding internal fields for the various types of P_s cells, we assume that the fields at the proton sites are primarily dipolar. The distribution of magnetization on the Mn ions is approximately spherically symmetric, and they may therefore be replaced with point dipoles. The magnitude of the moment of the dipoles is assumed to be five Bohr magnetrons at 0°K. The moment is assumed to have the same temperature dependence as the proton resonance frequencies. The moment found in this way may be the order of 3% too high because spin-wave corrections are neglected. The direction of the moments is taken as the hard axis χ_{11} of the *antiferromagnetic* susceptibility tensor. Smith and Friedberg[14] indicate that this axis is approximately along the O-Mn-O direction. The results of Cowen[15] and Fairall place the axis 10° from the O-Mn-O direction with an orientation with respect to crystallographic axes a, b, and c given by the angles $\alpha_0=57°$, $\beta_0=48°$, and $\gamma_0=38°$ for both the Rb and Cs compounds. The latter orientation is more consistent with our Cl-resonance data, and we have therefore used it in the present calculations. Fortunately, the results for the protons are not extremely sensitive to which of the two directions is chosen as the direction of magnetization. The position of the proton was located by using the hydrogen-bonding scheme given by Jensen[16] and the O-H distance of 0.987 Å suggested by El Saffar.[17] This technique for locating the proton positions seems to give reasonably reliable results in the few cases where it has been checked by neutron diffraction (e.g., $MnCl_2\cdot 4H_2O$). Numerical checks show that the computed fields are rather insensitive to small errors in the proton positions. The actual dipolar sums used in computing the internal fields extended over 1000 Mn ions. Of the seven types of P_s cells examined in the computations, only those containing $a+b$ or b antitranslations gave any measure of agreement with the experimental internal fields. The orientation and magnitude errors for the cell containing only the b antitranslation are roughly twice as large as for the cell with the $a+b$ antitranslation. The fields computed for the latter type of cell are compared with the experimental results in Table III. The rather large differences ($\sim 10\%$) between the magnitude of the calculated and observed internal fields may arise from the fact that the proton positions are only approximately known. However, differences nearly this large are encountered in $MnCl_2\cdot 4H_2O$,[18] where the proton positions are accurately known from neutron diffraction. One likely source of the discrepancies between the observed and calculated proton internal fields is the presence of unpaired spin density on the oxygen ion. One percent of an unpaired spin on the oxygen ion would produce a dipolar field of the order of 200 Oe at the proton sites. Experiments on the O^{17} nuclear resonance would be of considerable interest in all the hydrated antiferromagnetics. The relation of the chemical unit cell and the magnetic unit cell is shown in Fig. 4.

C. Chlorine Resonance

In both of these crystals one observes six Cl^{35} and six Cl^{37} lines in the antiferromagnetic state. The temperature dependence of the Cl^{35} lines is shown in Figs. 5 and 6. The pure quadrupole resonance frequencies are also shown for temperatures above T_N. The first problem is to separate the six lines into two groups of three lines associated with the two distinct pure quadrupole frequencies and the two chlorine sites in the crystal. To carry out this sorting process we invoke two criteria:

(a) Given an assumed set of lines and an assumed assignment to the three $\Delta m=\pm 1$ transitions, one may

TABLE III. Comparison of experimental proton fields with those calculated on the basis of an $a+b$ antitranslation.

Compound	Proton site		Orientation[a] α	β	γ	Magnitude (kOe at 1.1°K)
$Rb_2MnCl_4\cdot 2H_2O$	1	Expt.	59°	30°	54°	4.45
	1	Calc.	58°	34°	51°	4.14
	2	Expt.	36°	66°	53°	4.30
	2	Calc.	36°	72°	52°	4.37
$Cs_2MnCl_4\cdot 2H_2O$	1	Expt.	53°	35°	56°	4.08
	1	Calc.	57°	33°	53°	3.72
	2	Expt.	30°	75°	58°	4.02
	2	Calc.	34°	71°	54°	3.84

[a] Angles with respect to crystallographic axes.

[14] S. A. Friedberg (private communication).
[15] J. A. Cowen (private communication).
[16] See Ref. 5.
[17] Z. M. El Saffar, J. Chem. Phys. **45**, 4643 (1966).
[18] R. D. Spence and V. Nagarajan, Phys. Rev. **149**, 191 (1966).

TABLE IV. Assignment of Cl^{35} lines in $Rb_2MnCl_4 \cdot 2H_2O$.

ν_i[a] Mc/sec	$\frac{2\pi}{\gamma}\lvert\nabla_H\nu_i\rvert$	Orientation[b] of $\nabla_H\nu_i$ α_i	β_i	γ_i	Transition[c]	Pure quad. freq. ν_p	Site
10.715	1.13	67°	34°	40°	$\frac{3}{2} \leftrightarrow \frac{1}{2}$		
8.560	1.08	60°	48°	35°	$-\frac{1}{2} \leftrightarrow \frac{1}{2}$	3.854	Cl_{II}
6.250	1.20	71°	69°	17°	$-\frac{3}{2} \leftrightarrow -\frac{1}{2}$		
10.480	1.14	48°	59°	41°	$\frac{3}{2} \leftrightarrow \frac{1}{2}$		
9.635	1.05	50°	61°	38°	$-\frac{1}{2} \leftrightarrow \frac{1}{2}$	5.335	Cl_I
7.725	1.20	77°	26°	42°	$-\frac{3}{2} \leftrightarrow -\frac{1}{2}$		

[a] At 1.1°.
[b] Angles with respect to crystallographic axes.
[c] $\frac{3}{2} \leftrightarrow \frac{1}{2}$ and $-\frac{3}{2} \leftrightarrow -\frac{1}{2}$ transitions may be interchanged.

use Eq. (10) to compute Γ_2 at each temperature. We also have from Eq. (6)

$$\Gamma_2 = 5(\gamma_n/2\pi)^2 B^2 + \nu_p^2, \tag{30}$$

where $\nu_p = \nu_Q(1+\eta^2/3)^{1/2}$ is the pure quadrupole frequency. Since all internal fields should have the same temperature dependence, plotting Γ_2 as a function of the proton frequency squared should give a straight line with an intercept corresponding to one of the pure quadrupole frequencies observed in the paramagnetic state. While this criterion serves to eliminate a large number of possible sets of lines, it is not completely satisfactory, since neither the proton nor chlorine lines can be observed close to the Néel temperature, and thus the extrapolation of the straight line to ν_p^2 is somewhat uncertain. To choose among the assignments which can not be rejected on the basis of criterion (a), we employ criterion (b).

(b) Consider the situation in which $\eta = 0$ and only the $\Delta m = \pm 1$ transitions are of observable intensity (i.e., $B > 2\pi\nu_p/\gamma_n$). The three vectors $\nabla_H\nu_i$ originating from a given Cl site will be exactly coplanar with each other and with the vector B and the Z axis of the electric-field

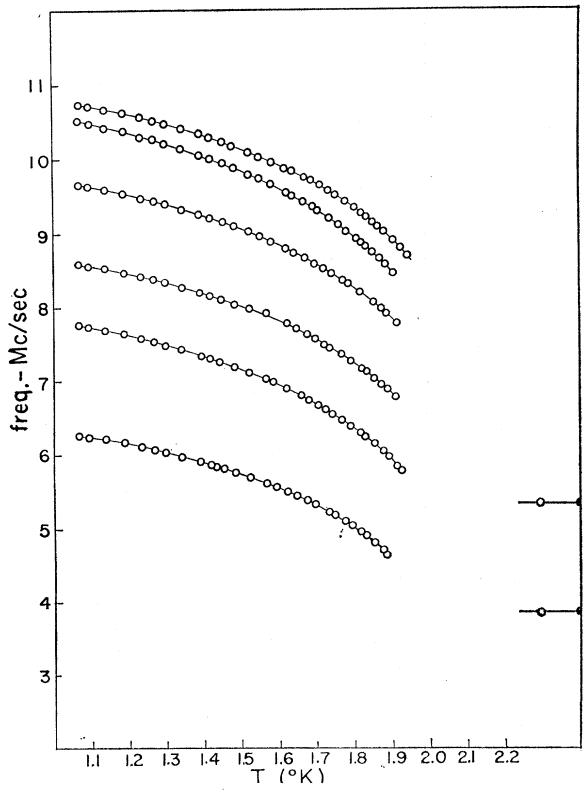

FIG. 5. Temperature dependence of the Cl^{35} lines in $Rb_2MnCl_4 \cdot 2H_2O$.

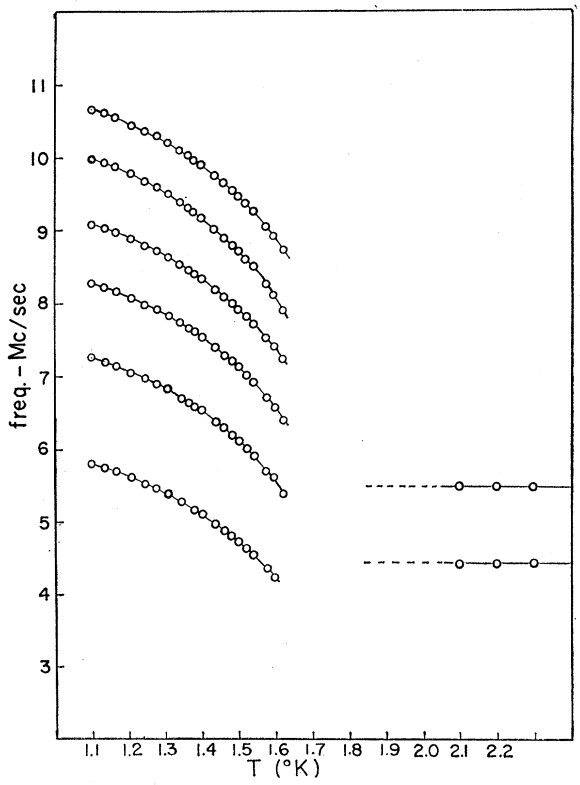

FIG. 6. Temperature dependence of the Cl^{35} lines in $Cs_2MnCl_4 \cdot 2H_2O$.

TABLE V. Assignment of Cl^{35} lines in $Cs_2MnCl_4 \cdot 2H_2O$.

ν_i[a] Mc/sec	$\frac{2\pi}{\gamma}\lvert\nabla_H\nu_i\rvert$	Orientation[b] of $\nabla_H\nu_i$ α_i	β_i	γ_i	Transition[c]	Pure quad. freq. ν_p	Site
10.670	1.24	68°	29°	45°	$\frac{3}{2} \leftrightarrow \frac{1}{2}$		
8.280	1.15	54°	46°	43°	$-\frac{1}{2} \leftrightarrow \frac{1}{2}$	4.433	Cl_{II}
5.805	1.36	73°	77°	18°	$-\frac{3}{2} \leftrightarrow -\frac{1}{2}$		
10.000	1.23	45°	62°	43°	$\frac{3}{2} \leftrightarrow \frac{1}{2}$		
9.095	1.14	49°	65°	39°	$-\frac{1}{2} \leftrightarrow \frac{1}{2}$	5.497	Cl_I
7.265	1.46	83°	16°	51°	$-\frac{3}{2} \leftrightarrow -\frac{1}{2}$		

[a] At 1.1°K.
[b] Angles with respect to crystallographic axes.
[c] $\frac{3}{2} \leftrightarrow \frac{1}{2}$ and $-\frac{3}{2} \leftrightarrow -\frac{1}{2}$ transitions may be interchanged.

gradient. The $-\frac{1}{2} \leftrightarrow \frac{1}{2}$ transition will be identifiable from the fact that the direction of its gradient will be closest to the gradient of the high-frequency line and the magnitude of its gradient will be smaller than that of the other two lines. If η is nonzero but not too large, one may show by using perturbation theory expansions that the three $\nabla_H\nu_i$ are still approximately coplanar but their plane is tilted with respect to the plane of $\mathbf{B}$ and Z. The $-\frac{1}{2} \leftrightarrow \frac{1}{2}$ transition will be identifiable as before over a considerable range of nonzero η.

Using the two criteria the Cl^{35} lines of the two compounds are assigned as in Tables IV and V. The Z axes of the electric-field gradients of the two Cl sites are expected to be near the corresponding Mn-Cl bond directions. Applying the approximate coplanar condition given in (b) to the stereograms in Figs. 7 and 8 leads to the association between sets of lines and Cl sites given in Tables IV and V. The consistency of this assignment may be checked by computing the angle between the Z axis and direction of $\mathbf{G}_2$ (or $\mathbf{B}$). We find that the angle between the Mn-Cl bond and the Z axis is 9° for Cl_I and 6° for Cl_{II}.

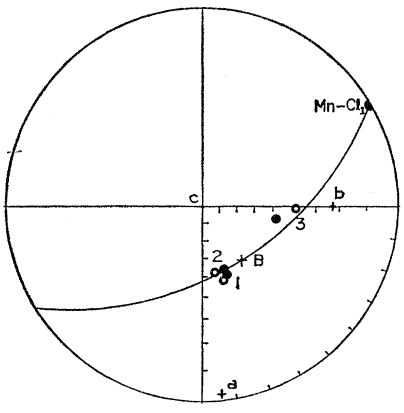

FIG. 7. Orientation of the $\nabla_H\nu_i$ vectors for Cl_I sites. Black circles for $Rb_2MnCl_4 \cdot 2H_2O$. Open circles for $Cs_2MnCl_4 \cdot 2H_2O$. The numbers refer to the frequencies as listed in Tables IV and V, i.e., 1 for highest frequency, 3 for lowest frequency. The plane passing through B and the Mn-Cl_I direction is the plane in which the vectors would lie *if* η were zero and the Z axis of ∇E were exactly along Mn-Cl_I.

The hyperfine fields $\mathbf{B}_h$ computed from the previous assignment are given in Table VI. They lie within 2° of the direction of $\mathfrak{y}$ as given by Cowen and Fairall. This is not too surprising, since the hyperfine tensors of the manganese salts are quite isotropic, presumably due to nearly equal amounts of unpaired spin in the π bonds and σ bond. Since the dipolar field $\mathbf{B}_d$ which must be subtracted from $\mathbf{B}$ to obtain $\mathbf{B}_h$ is small and does not vary rapidly with the orientation of $\mathfrak{y}$ our results indicate that the direction of $\mathfrak{y}$ given by Cowen and Fairall is probably correct.

The difference in orientation of $\mathbf{B}_h$ for the Cl_I and Cl_{II} sites, which is shown in Table VI, scarcely exceeds the experimental error. However, the remarkable consistence of the two compounds with respect to this difference strongly suggests that the axes of the hyperfine tensors are different for the two sites. This is further supported by comparing the values of A_e. The values of A_e for Cl are the same to within experimental error in the two compounds. The slight difference in A_e for the Cl_{II} sites probably only reflects the fact that the Mn-Cl_{II} distance is 2.58 Å in $Rb_2MnCl_4 \cdot 2H_2O$ as compared with 2.54 Å in $Cs_2MnCl_4 \cdot 2H_2O$. The main conclusion which seems to appear from comparison of the

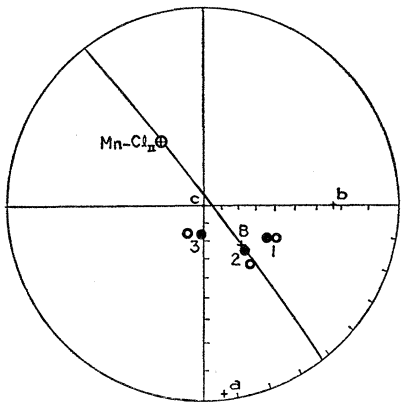

FIG. 8. Orientation of the $\nabla_H\nu_i$ vectors for Cl_{II} sites. Labelling conventions are the same as in Fig. 7, but here the plane is orientated to represent the vectors as they would lie *if* η were zero and the Z for this set were exactly along Mn-Cl_{II} direction.

TABLE VI. Cl^{35} hyperfine fields.

Compound	Site	B_h (kOe at 1.1°K)	Orientation[a] α	β	γ	Λ_e[b]	A_e (10^{-4} cm^{-1})
$Rb_2MnCl_4\cdot 2H_2O$	Cl_I	24.76	55°	49°	40°	5.65	1.46
	Cl_{II}	22.03	59°	49°	36°	5.08	1.30
$Cs_2MnCl_4\cdot 2H_2O$	Cl_I	23.10	55°	48°	40°	5.68	1.47
	Cl_{II}	21.36	59°	49°	36°	5.25	1.36

[a] Angles with respect to crystallographic axis.
[b] Units are Å^{-3}.

Cl hyperfine effects in the two salts is that they do not reflect the difference in the Néel temperature. The values of A_e are in good agreement with the values of A found for $MnCl_2\cdot 4H_2O$.[19]

D. Rubidium Resonance in $Rb_2MnCl_4\cdot 2H_2O$

At temperatures above T_N we observe three pure quadrupole resonance lines which arise from the Rb^{85} and Rb^{87} isotopes. Table VII gives the assignment of these lines and the frequencies at which they were observed in the temperature range from T_N to 3.0°K. The assignment in Table VII is based on the following arguments. Using this assignment one finds for the ratio of $R_Q=Q_{5/2}/Q_{3/2}=2.07\pm0.06$, which is in good agreement with the value $R_Q=2.0669\pm0.0005$ obtained by Meyer-Berkhout[20] using beam techniques. Alternative assignments except those which merely interchange ν_I and ν_{II} do not lead to agreement on the value of R_Q. Furthermore, the assignment is one which leads to continuity with the Rb^{85} and Rb^{87} lines observed in the antiferromagnetic state. The asymmetry parameter η was calculated using Eqs. (6) and (7) which for $B=0$ yields

$$(1+\eta^2/3)^3/(1-\eta^2)^2=(25/1029)[(\Gamma_2{}^p)^3/(\Gamma_3{}^p)^2]. \quad (31)$$

Using the frequencies given in Table VII to evaluate the expression leads to $\eta=0.78$. Alternatively, one may use the tables of Livingston and Zeldes[21] to obtain a value of η for which the ratio ν_I/ν_{II} corresponds to that experimentally observed. This gives the same value of η.

Figure 9 shows the temperature dependence of the Rb^{87} frequencies in the *antiferromagnetic* state. Six lines are observed. If we designate the frequencies of these lines $\nu_1>\nu_2>\nu_3>\nu_4>\nu_5>\nu_6$, we find

$$\nu_1=\nu_2+\nu_3=\nu_3+\nu_4,$$
$$\nu_6=\nu_2-\nu_4=\nu_2-\nu_5.$$

These relations are satisfied by the energy-level scheme shown in Fig. 10. The magnitude of the internal field at the Rb sites at each temperature may be found by using Eq. (13). Figure 11 shows the energy levels as a function of the *internal field*. This figure was constructed by converting the frequencies versus temperature curves of Fig. 9 to energy-versus-temperature curves (using the condition that the Hamiltonian is traceless) and then replotting the result, using the experimental relations between the internal field and temperature.

TABLE VII. Pure quadrupole lines of Rb^{85} and Rb^{87}.

Isotope	Spin	Transition	Freq. (Mc/sec at 3.0°K)
Rb^{85}	$\frac{5}{2}$	$\nu_I=\pm\frac{3}{2}\leftrightarrow\pm\frac{1}{2}$	2.6743±0.0018
		$\nu_{II}=\pm\frac{5}{2}\leftrightarrow\pm\frac{3}{2}$	3.2229±0.0060
Rb^{87}	$\frac{3}{2}$	$\nu_0=\pm\frac{3}{2}\leftrightarrow\pm\frac{1}{2}$	3.1161±0.0016

[19] See Ref. 18.
[20] U. Meyer-Berkhout, Z. Physik **141**, 185 (1955).
[21] R. Livingston and H. Zeldes, Oak Ridge National Report No. ORNL-1913, 1955 (unpublished).

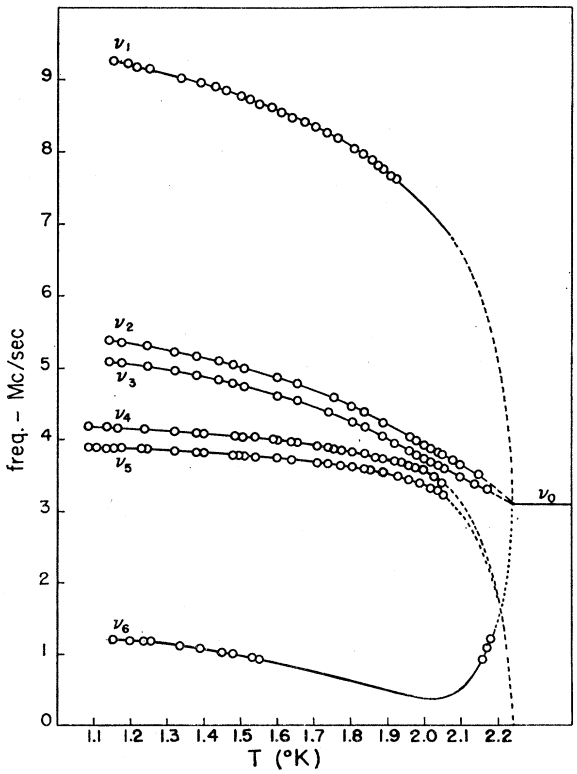

FIG. 9. Temperature dependence of the Rb^{87} lines.

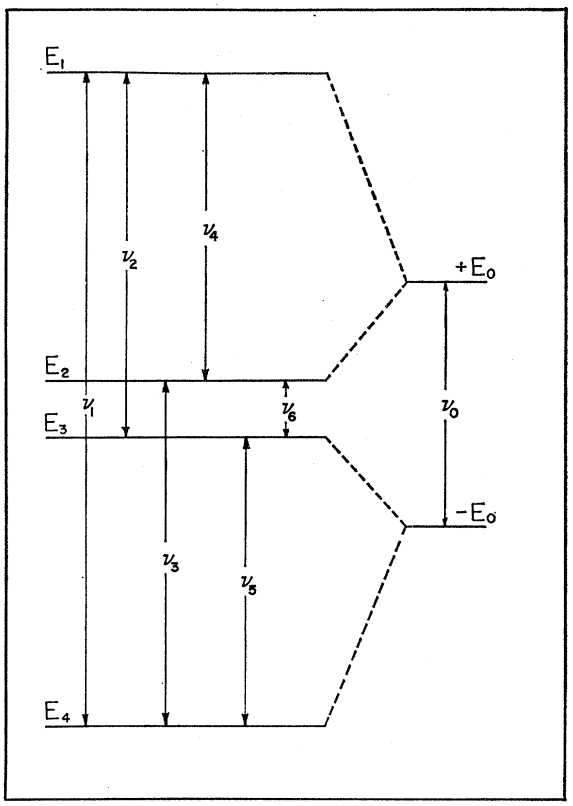

FIG. 10. Energy levels and transitions observed for Rb^{87}.

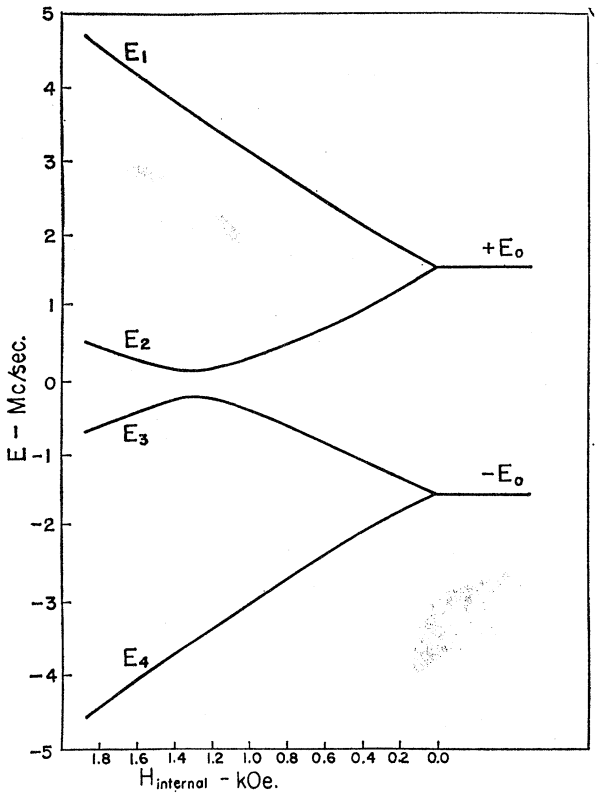

FIG. 11. Energy levels for Rb^{87} as a function of the internal field.

The temperature dependence of the Rb^{85} lines in the antiferromagnetic state is shown in Fig. 12. The small temperature dependence of these lines reflects the fact that $\gamma^{85}/\gamma^{87}=0.2951$. The appearance of the square of this factor in the ratio of transition probabilities probably accounts for the fact that the Rb^{85} lines are of lower intensity than those of Rb^{87} even though the abundance ratio is 2.65:1. Only lines which in the low-field notation correspond to $\Delta m=\pm 1$ transitions were observed for the Rb^{85}.

The orientation of the internal fields at the Rb site was obtained by measuring the $\mathbf{G}_2$ vector in the same manner as at the Cl sites. The orientation found in this way was checked to a certain extent by the following technique: Since Γ_3 and η are known experimentally, a cone $\theta=\theta(\varphi)$ is specified on which the internal field must lie. The angles θ and φ are measured with respect to the axes of the electric field gradient. These axes were found by measurements in the paramagnetic state. To within experimental error the $\mathbf{G}_2$ vector lies on the surface of the cone obtained by these measurements.

E. Cesium Resonance in $Cs_2MnCl_4\cdot 2H_2O$

The Cs^{133} resonance in the antiferromagnetic state consists of seven closely spaced lines as are shown in Fig. 13. The temperature dependence of these lines is shown in Fig. 14. For this nucleus the pure quadrupole resonances are so low in frequency that a separate experiment was carried out in the paramagnetic state at a field of 6000 Oe to enable us to calculate $\Gamma_2{}^p$. Using this result and the value of $\Gamma_2{}^a$ from the antiferromagnetic data enabled us to calculate the magnitude of the internal field. The experiments in the paramagnetic

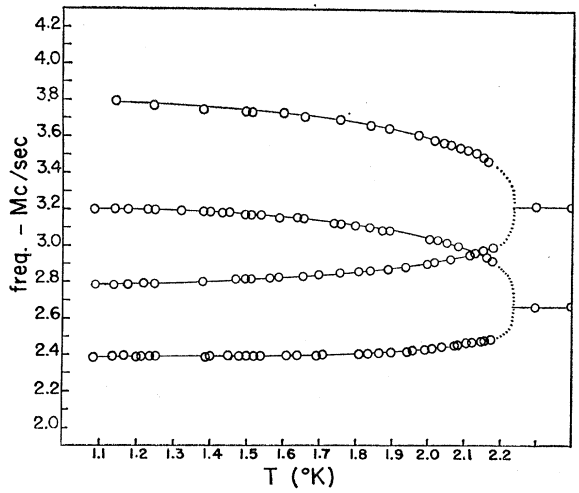

FIG. 12. Temperature dependence of the Rb^{85} lines.

TABLE VIII. Hyperfine fields at Rb and Cs sites.

Site	Orientation[a] α	β	γ	Magnitude (kOe at 1.1°K)	Λ_c[b]
Rb	55°	42°	47°	0.884	0.20
Cs	53°	42°	48°	1.442	0.35

[a] Angles with respect to crystallographic axes.
[b] Units are $Å^{-3}$.

state also gave a value for the asymmetry parameter ($\eta=0.80$) and the axes of the electric field gradient. The orientation of the latter are not the same as in $Rb_2MnCl_4 \cdot 2H_2O$. The direction of the Z axis differs by 9° in the two compounds. This immediate environment of the Rb or Cs ions in these compounds is a set of eight Cl ions arranged in a slightly distorted cesium chloride structure. The fact that the distortions vary in different ways may explain the difference in the axes of the electric-field gradient. The orientation of the internal fields was determined by the $\mathbf{G}_2$ vector and again checked to see if it lay on the $\theta=\theta(\varphi)$ cone. The reason for carrying out these checks for the Rb and Cs sites can be explained by our discovery that the orientation of the $\mathbf{G}_2$ vectors was quite different for the two nuclei. However, when the dipolar fields were subtracted, it was found (see Table VIII) that to within experimental error the hyperfine fields at the Rb and Cs sites had the same orientation. Furthermore, although the orientation of these fields is quite close to those at the Cl sites, the difference is large enough to indicate that there is a difference in the orientation of the axes of the hyperfine tensors at Cl and Rb (or Cs) sites. The magnitude of the hyperfine field at the Cs site is considerably larger than at a Rb site even though the Mn-Cs distances are larger than the Mn-Rb distances. Apparently this difference arises from the difference in the radial extent of $5s$ and $5p$ wave functions of Cs compared to the $4s$ and $4p$ wave functions of Rb.

There are three nearest-neighbor Mn ions at distances 4.18, 4.21, and 4.38 Å from the Rb site. The space group, which we have found from the proton-resonance data, requires that two of the spins on the nearest-neighbor Mn ions have the same orientation and the third be oppositely directed. Using Eq. (23), one may calculate an *average* value of A_e for the Rb^{87} interaction. We find $A_e^{87}=0.17\times10^{-4}$ cm^{-1} which may be compared with $A^{87}=0.12\times10^{-4}$ cm^{-1} found in $RbMnF_3$ by Payne *et al.*[22] and Petrov *et al.*[23]

IV. MAGNETISM AND CRYSTAL STRUCTURE

The increase in the Néel temperature, which occurs on replacing Cs with Rb in these compounds, probably

[22] R. E. Payne, R. E. Forman, and A. H. Kahn, J. Chem. Phys. 42, 3806 (1965).
[23] M. P. Petrov, G. S. Smolenskii, and P. P. Syrnikov, Fiz. Tverd. Tela 7, 3689 (1965) [English transl.: Soviet Phys.—Solid State 7, 2984 (1966)].

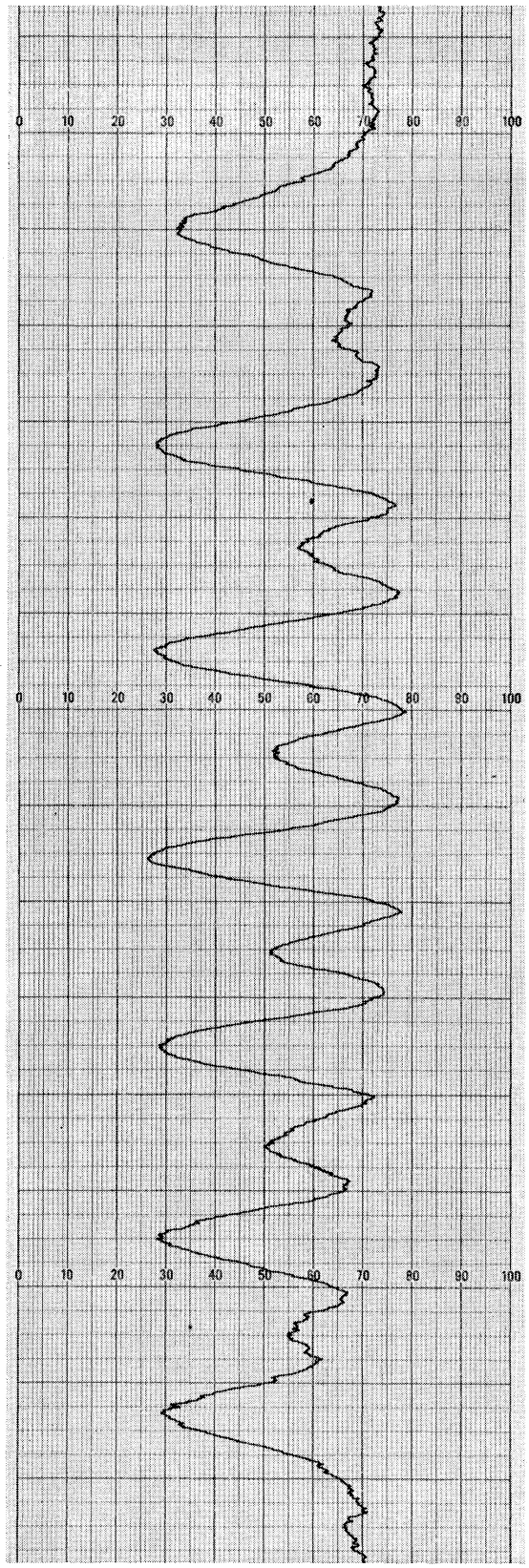

FIG. 13. Recording of the Cs^{133} lines in the antiferromagnetic state ($T=1.1$°K). Second-derivative detection is used.

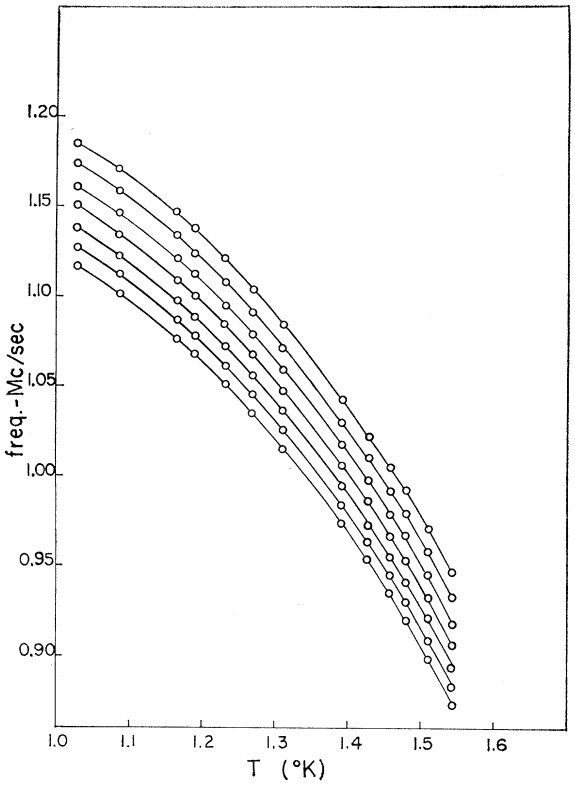

FIG. 14. Temperature dependence of the Cs^{133} lines.

arises from the decrease in the dimensions of the unit cell. The decrease in T_N is somewhat smaller than might have been expected on the basis of the reduction of the Mn-Mn distances alone. According to Anderson[24] the proper wave function for the magnetic electrons consists of d wave functions with appropriate admixtures from all the ligands. The presence of an appreciable hyperfine field at the Rb and Cs sites indicates that admixtures from ions not directly bonded to the magnetic ion should be included in the magnetic wave function. Since the hyperfine field at the Cs site is larger than at the Rb site, it appears possible that increased admixture with the Cs electrons inhibited somewhat the reduction in T_N, which its larger ionic radius might have otherwise produced.

The considerable difference in the hyperfine fields at the two Cl sites emphasizes the fact that the Mn-O axis of the coordination octahedron is not a fourfold axis, although the crystallographic distortions appear to be quite small. In view of this fact, it is not too surprising that the magnetization direction is shifted from the Mn-O direction.

Hydrogen bonding occurs in the a-b plane of these crystals. This is also the plane of the antiferromagnetic exchange as indicated by the antitranslations found from proton resonance. It is not clear whether this correlation is merely a result of reduced Mn-Mn spacing in these dimensions or whether the hydrogen bond can play a direct role in the exchange process. The latter idea has been suggested by Haseda.[25] Experimentally it has been shown that replacing the protons with deuterons in $CoCl_2 \cdot 6H_2O$ shifts[26] T_N and changes the orientation of the Cl hyperfine fields.[27]

ACKNOWLEDGMENTS

The authors wish to thank Professor J. A. Cowen of Michigan State University and Professor S. A. Friedberg of the Carnegie-Mellon University for communicating their data on the susceptibility of these compounds. We wish also to thank Professor H. Forstat, Professor P. Parker, and Dr. E. Carlson for valuable suggestions. We are also much indebted to W. deJonge for his considerable help in collecting the data.

[24] P. W. Anderson, in Ref. 11, Vol. I, Chap. 2.

[25] T. Haseda, J. Phys. Soc. Japan **15**, 483 (1960).

[26] D. S. Sahri and M. Bloom, Phys. Rev. **159**, 482 (1967).

[27] J-P. Legrand and J-P. Renard, Compt. Rend. **266**, Ser. B, 1165 (1968).

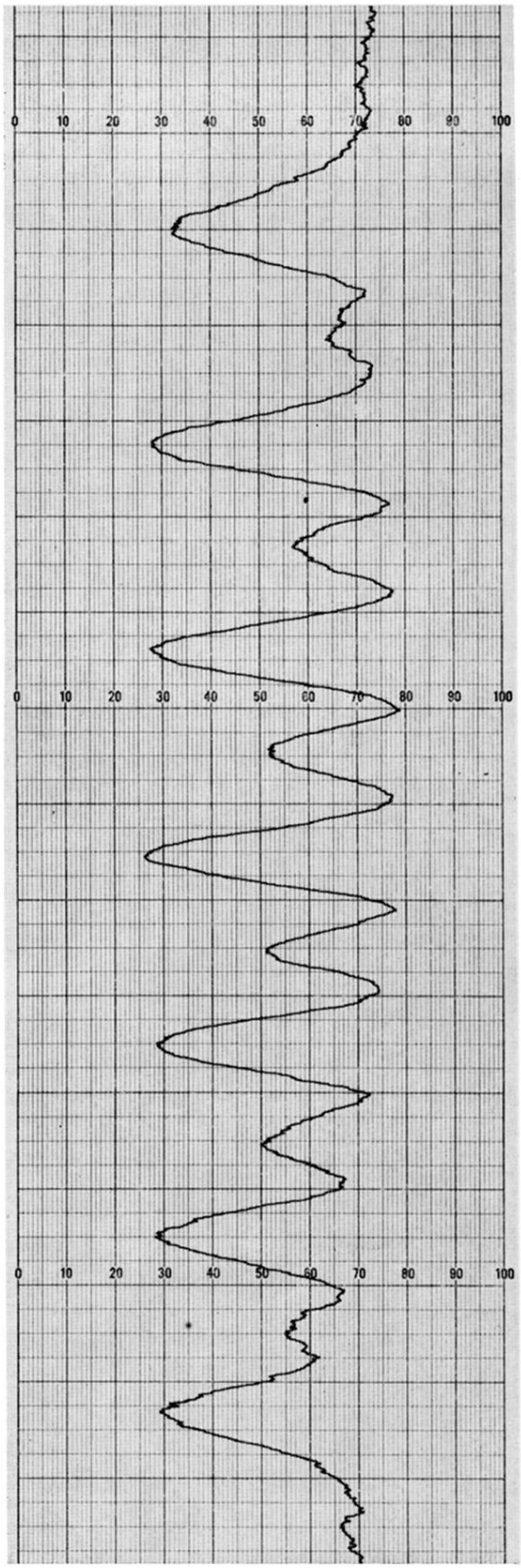

FIG. 13. Recording of the Cs^{133} lines in the antiferromagnetic state ($T=1.1°K$). Second-derivative detection is used.